Clays and Clay Minerals, Vol. 68, No. 5:436–445, 2020

ENERGY MODELING OF COMPETITION BETWEEN TUBULAR AND PLATY MORPHOLOGIES OF CHRYSOTILE AND HALLOYSITE LAYERS

Andrei A. Krasilin*
[1]Ioffe Institute, 26 Politekhnicheskaya st., St. Petersburg 194021, Russia

Abstract—The present study considered the problem of halloysite nanoscroll synthesis by energy modeling of the formation of chrysotile and halloysite particles. The main aim of the study was to reveal an energy preference between scrolled and platy morphologies of the particles. Both hydrosilicates possess the ability to scroll spontaneously but relatively facile hydrothermal synthesis of the nanoscrolls is available only to the former, whereas halloysite forms mainly plates under the same conditions. This issue was investigated by a phenomenological energy model, taking into account: (1) strain energy due to the size difference between metal oxide and silica sheets; (2) surface-energy difference on the opposite sides of the layer; and (3) adhesion energy. Calculations showed that the halloysite layer had a significant scrolling potential due to the first energy component, but the surface-energy difference acted in the opposite direction and tried to unbend the layer. In contrast, these two actions were co-directional in chrysotile layers. In both cases, the formation of multi-layered plates became more energy favorable when the specific surface energy of the edges decreased. In the range 0.5–3 J/m^2 for the specific surface energy, only halloysite layers showed an energy preference for platy particles over nanoscrolls, especially at small layer sizes. Certain processes, such as hydration, could reduce the corresponding specific surface energy value and, as a result, could stabilize the platy morphology of halloysite at the earliest stages of particle growth under hydrothermal conditions.

Keywords—Chrysotile · Energy modeling · Halloysite · Nanoscroll · Nanotube · Surface energy

INTRODUCTION

The last decade (2010–2020) has been marked by a new wave of interest in clays and clay minerals. Many applications have been found, in fields ranging from adsorption and water remediation to catalysis and medicine, and these are due to the natural abundance and morphological and structural diversity of clay minerals. Among these minerals, hydrosilicates are an interesting group which are able to scroll spontaneously: $Al_2SiO_3(OH)_4$ imogolite (Paineau et al. 2016; Shafia et al. 2016; Arancibia-Miranda et al. 2017; Picot et al. 2018), $Mg_3Si_2O_5(OH)_4$ chrysotile (Bloise et al. 2010; Korytkova et al. 2011; Lafay et al. 2016; Krasilin et al. 2017; Maslennikova and Gatina 2017; López-Salinas et al. 2019; Bian and Kawi 2020), and $Al_2Si_2O_5(OH)_4$ halloysite (Cataldo et al. 2018; Krasilin et al. 2019b; Lvov et al. 2019). Their crystal structures combine two covalently bonded sheets of metal-oxygen octahedra and silicon-oxygen tetrahedra (joined in a network or separated as in the case of imogolite). Substantial differences in the size of the sheets and in terms of their structure give rise to a bending momentum, which transforms the layers into single-walled or multi-walled tubular, conical (Bloise et al. 2009b; Krasilin et al. 2015), or even spheroidal (Berthonneau et al. 2015; Cravero et al. 2016; Thill et al. 2017; Du et al. 2020) particles. This intriguing structural feature has led to theoretical research based on the density functional theory method (Guimarães et al. 2010; Lourenço et al. 2012; da Silva et al. 2015; Poli et al. 2015, 2016; Demichelis et al. 2016), molecular dynamics (Prishchenko et al. 2018; Gonzalez et al. 2018), hydrodynamics (Chivilikhin et al. 2007), and phenomenological modeling (Singh 1996; Perbost et al. 2003; Chivilikhin et al. 2009; Thill et al. 2012; Krasilin and Gusarov 2014). Most tubular minerals can be synthesized successfully in the laboratory using soft chemical and hydrothermal techniques; this is not true of halloysite.

Few reports about the hydrothermal synthesis of tubular halloysite can be found in the literature (White et al. 2012) and those mention the very small yield of nanotubes and nanoscrolls in comparison to platy particles. To date, the principal approach to producing tubular halloysite has been exfoliation of its platy analog, kaolinite (Kuroda et al. 2011; Liu et al. 2016; Makó et al. 2017; Zsirka et al. 2017; Li et al. 2019), and most of the application-oriented studies have involved mined halloysite (Cavallaro et al. 2017; Ma et al. 2018; Goda et al. 2019). Theoretical research on the halloysite layer (Guimarães et al. 2010; Ferrante et al. 2015; Prishchenko et al. 2018) has confirmed its significant scrolling potential. Chrysotile layers, which have a very similar structure, scroll with ease in hydrothermal conditions.

In previous studies, an energy model of multi-walled nanoscroll formation was developed by Krasilin and Gusarov (2015, 2016). The model explained $(Mg,Ni)_3Si_2O_5(OH)_4$ diameter and length distributions of the nanoscrolls (Krasilin et al. 2017), as well as the increase in the amount of conical nanoscrolls (Krasilin and Gusarov 2017). For the present study, the model was applied to a description of the energy effect of multi-walled plate formation of chrysotile and halloysite followed by comparison with the energy effect of scrolling of corresponding layers. The main purpose was to unearth hindrances which prevent halloysite particles from spontaneous scrolling in artificial hydrothermal conditions.

* E-mail address of corresponding author: ikrasilin@mail.ioffe.ru
DOI: 10.1007/s42860-020-00086-6

THEORY

Energy Effect of Scrolling

The energy model consists of a layer composed of two sheets of different size and structure (Fig. 1a). These differences initiate the scrolling. The energy effect of scrolling is written as follows:

$$\Delta E_{/}^{@} = \frac{1}{\nu}\left[\left(E_s^{@} - E_s^{/}\right) + \left(\Sigma^{@} - \Sigma^{/}\right) - U_a^{@}\right] \quad (1)$$

where ν is the amount of substance, $E_s^{@}$ and $E_s^{/}$ are strain energies of the scrolled (@) and flat (/) layers, $\Sigma^{@}$ and $\Sigma^{/}$ are surface energies of the scrolled and flat layers, and $U_a^{@}$ is the adhesion energy of a multi-walled scroll.

Assuming that a nanoscroll cross-section can be described by the Archimedean spiral, $E_s^{@}$ is expressed through integration in polar coordinates:

$$E_s^{@} = \frac{D_s}{2} L_2 \int_0^{2\pi n} \left(\frac{1}{r(\varphi)} - \frac{1}{r_0}\right)^2 \sqrt{f^2 + r^2(\varphi)}\, d\varphi \quad (2)$$

where D_s is bending stiffness, L_2 is the length of the scroll (i.e. length of the cylinder), n is the number of layers within the wall, $r(\varphi)$ is the current radius, r_0 is the radius of the mechanically unstressed layer, and f is the spiral constant. The part under the square root is the length of the integration element, which yields the spiral length after integration.

If the layer can be described using the continuous mechanics approach (Landau et al. 1986), the bending stiffness can be shown as:

$$D_s = \frac{Yh^3}{12(1-\mu^2)} \quad (3)$$

where Y is Young's modulus of the layer, h is the thickness of the layer, and μ is the Poisson ratio.

The Archimedean spiral attributes are:

$$\begin{aligned} r(\varphi) &= r_{in} + f\varphi \\ f &= \frac{h+t}{2\pi} \end{aligned} \quad (4)$$

where r_{in} is the inner (initial) radius of the scroll and t is the interlayer spacing.

The r_0 value depends on size of the sheets (Fig. 1b):

$$r_0 = \frac{h}{4}\frac{b_{out} + b_{in}}{b_{out} - b_{in}} \quad (5)$$

where b_{out} and b_{in} are the size of the outer and inner sheets, respectively, i.e. lattice constants.

The r_0^{chr} value of $Mg_3Si_2O_5(OH)_4$ chrysotile is well known (Cressey and Whittaker 1993; Demichelis et al. 2016), and one could estimate r_0^* for some scrolls of another chemical composition. Assuming constant layer thickness, the size of the tetrahedral sheet and the direction of the new scrolling r_0^* value is:

$$r_0^* = \frac{h}{4}\frac{b^*\left(r_0^{chr} + h/4\right) + b^{Mg}\left(r_0^{chr} - h/4\right)}{b^*\left(r_0^{chr} + h/4\right) - b^{Mg}\left(r_0^{chr} - h/4\right)} \quad (6)$$

where b^* is proportional to the lattice constant of metal hydroxide and b^{Mg} is proportional to the lattice constant of $Mg(OH)_2$. In cases where the direction of scrolling is opposite to that of chrysotile:

$$r_0^* = \frac{h}{4}\frac{b^{Mg}\left(r_0^{chr} - h/4\right) + b^*\left(r_0^{chr} + h/4\right)}{b^{Mg}\left(r_0^{chr} + h/4\right) + b^*\left(r_0^{chr} - h/4\right)} \quad (7)$$

Note that b^{Mg} and b^* must correspond with each other in terms of an equal number of polyhedra (Fig. 1a).

The strain energy of the flat layer is:

$$E_s^{/} = \frac{D_s}{2r_0^2} L_1 L_2 \quad (8)$$

where L_1 is the length of the flat layer along the direction of scrolling, which is equal to spiral length.

The surface energy of a scroll is the sum of all surface areas multiplied by specific surface energy values:

$$\Sigma^{@} = \sigma_{out} L_{1,out}^{@} L_2 + \sigma_{in} L_{1,in}^{@} L_2 + 2\sigma_1 L_1 h + 2\sigma_2 L_2 h \quad (9)$$

where σ_{out}, σ_{in}, σ_1, and σ_2 are the specific surface energies of the outer, inner, and the two-edge surfaces, respectively.

The lengths $L_{1,out}^{@}$ and $L_{1,in}^{@}$ of the spirals formed by outer and inner surfaces are determined as follows:

$$\begin{aligned} L_{1,out}^{@} &= \int_0^{2\pi n} \sqrt{f^2 + (r_{in} + h/2 + f\varphi)^2}\, d\varphi \\ L_{1,in}^{@} &= \int_0^{2\pi n} \sqrt{f^2 + (r_{in} - h/2 + f\varphi)^2}\, d\varphi \end{aligned} \quad (10)$$

In the case of the flat layer, Eq. 9 is simplified to:

$$\Sigma^{/} = \sigma_{out} L_1 L_2 + \sigma_{in} L_1 L_2 + 2\sigma_1 L_1 h + 2\sigma_2 L_2 h \quad (11)$$

The last component of Eq. 1, the adhesion energy, can be estimated using the same principle if $n > 1$:

$$U_a^{@} = u_a L_2 \int_0^{2\pi(n-1)} \sqrt{f^2 + \left[r_{in} + \frac{h+t}{2} + f\varphi\right]^2}\, d\varphi \quad (12)$$

where u_a is the specific adhesion energy.

Specific surface and adhesion energy values are assumed to be independent of the radius of curvature. Usually the size effects must be taken into account if the radius is <1–2 nm (Tolman 1949; Dumitrică et al. 2002; Vollath et al. 2018; Holec et al. 2020).

https://doi.org/10.1007/s42860-020-00086-6 Published online by Cambridge University Press

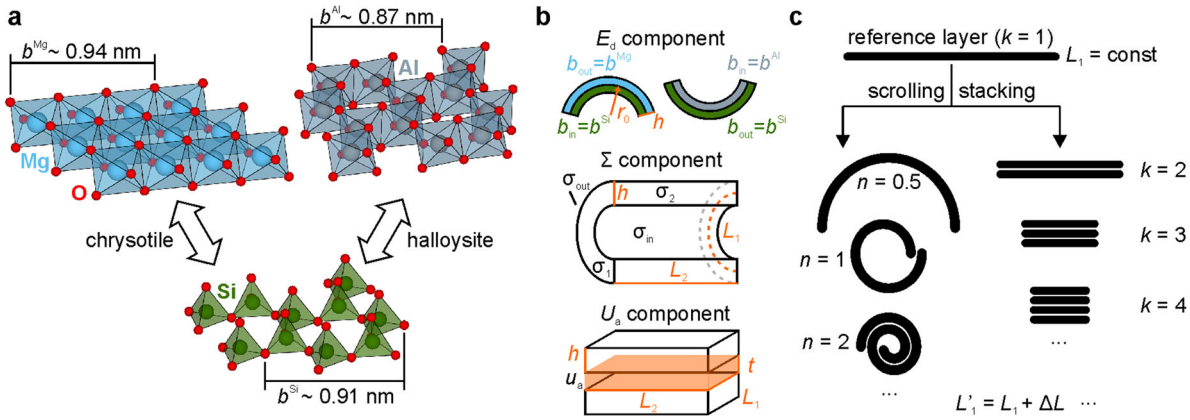

Fig. 1. Calculation concepts. **a** Covalent bonding of two different sheets yielded chrysotile and halloysite layers. Sheet structures were adopted from Saalfeld and Wedde (1974), Desgranges et al. (1996), Churakov et al. (2004), and Roveri et al. (2006) using *VESTA* software (Momma and Izumi 2011). **b** Structural parameters of the layers. **c** Scrolling and stacking of layers

Energy Effect of Multi-layered Plate Formation

A single flat layer of length L_1 can be divided into k equal parts (Fig. 1c), which are then stacked together to form a multi-layered rectangular plate. This procedure increases the surface energy of the plate due to the formation of new edge surfaces. On the other hand, the stacking of layers decreases their surface energy due to adhesion. As for strain energy, partition of the layer does not influence its value. Thus, the energy effect of multi-layered plate formation is:

$$\Delta E_{/}^{=} = \frac{1}{\nu}\left[\left(\Sigma^{=} - \Sigma^{/}\right) - U_{\mathrm{a}}^{=}\right] \tag{13}$$

The amount of substance, which is assumed to be constant during the scrolling process, can be calculated as follows:

$$\nu = \frac{L_1 L_2 h \rho}{M} \tag{14}$$

where ρ is the density of the layer and M is the molar mass.

The surface energy of the plate is:

$$\Sigma^{=} = \sigma_{\mathrm{out}} L_1 L_2 + \sigma_{\mathrm{in}} L_1 L_2 + 2\sigma_1 L_1 h + 2k\sigma_2 L_2 h \tag{15}$$

where $k = 1, 2, 3\ldots$

The adhesion energy when $k > 1$ is:

$$U_{\mathrm{a}}^{=} = u_{\mathrm{a}} L_1 L_2 \frac{k-1}{k} \tag{16}$$

The number of k layers stacked together in a plate is an integer equal to the number of layers, n. For the sake of comparison, the calculation results are represented in the same plots, considering $k = n$ where needed.

The specific adhesion energy, u_{a}, is calculated as the sum of hydrogen bond energies per unit area:

$$u_{\mathrm{a}} = \frac{\mathrm{C_K}\, N_{\mathrm{H}}\, \mathrm{C_W}}{\mathrm{N_A}\, ab\, t^{3.78}} \tag{17}$$

where $\mathrm{C_K}$ is a proportionality constant, $\mathrm{N_A}$ is Avogadro's number, N_{H} is the number of hydrogen bonds between adjacent hydrosilicate layers within one cell, a and b are lattice constants, and $\mathrm{C_W} = 1.2 \cdot 10^{10}$ (if t is expressed in pm) is the fitting constant proposed by Wendler et al. (2010).

Determination of Model Parameters

Equations 1 and 13 are solved numerically in order to find the energy effect of either multi-walled scroll or plate formation in comparison to a single flat layer of the same mass (Fig. 1). In Table 1 are given the numerical values of a number of structural parameters of the model. Chrysotile and halloysite scrolling directions are opposite (Krasilin et al. 2019b), so in order to estimate the r_0^{Al} value for halloysite, Eq. 7 is used, which yielded 3.3 nm. Remarkably, the same value was also obtained by solving an empirical equation proposed by Guimarães et al. (2010) as a fit of DFT calculations. Chrysotile and halloysite (7 Å modification) had almost equal layer thicknesses and interlayer spacings. Some previous theoretical and experimental results indicated that Young's moduli of the nanoscrolls were also similar (Piperno et al. 2007; Guimarães et al. 2010; Lourenço et al. 2012; Lecouvet et al. 2013); a significant scatter of experimental values was found, however. The influence of Young's modulus on the position and form of the multi-walled nanoscroll energy minimum can be found elsewhere (Krasilin and Gusarov 2016).

In order to assign specific surface energy values, the data for corresponding metal hydroxides and silica surfaces are used. The value of 3 meV/Å^2 (0.05 J/m^2) for the (0001) $Mg(OH)_2$ surface was used by Churakov et al. (2004); in the opinion of those authors, that value might have been an underestimate. For $Al(OH)_3$, the value of 0.22 J/m^2 for the (002) surface was used, obtained by Fleming et al. (2000). The choice of the σ value for the silica sheet surface was complicated by the fact that no close analogue has been found among

https://doi.org/10.1007/s42860-020-00086-6 Published online by Cambridge University Press

Table 1. Structural parameters of the energy model for chrysotile and halloysite layers

Parameter	Chrysotile	Halloysite	Reference
r_0 (nm)	8.8	3.3	Guimarães et al. (2010), Demichelis et al. (2016), present study
b^* (nm)	0.9438[a]	0.8684	Saalfeld and Wedde (1974), Desgranges et al. (1996), Churakov et al. (2004)
h (nm)	0.4	0.4	Roveri et al. (2006), Lvov et al. (2016), Krasilin et al. (2019a, b)
t (nm)	0.3	0.3	
Y (GPa)	300	300	Piperno et al. (2007), Guimarães et al. (2010), Lourenço et al. (2012), Lecouvet et al. (2013)
μ	0.2	0.2	Cressey and Whittaker (1993)
σ_{out} (J/m^2)	0.05[b]	1.51[c]	Shchipalov (2000), Churakov et al. (2004)
σ_{in} (J/m^2)	1.51[c]	0.22[d]	Fleming et al. (2000), Shchipalov (2000)
σ_e (J/m^2)	0.5–3.0[e]	0.5–3.0[e]	Fleming et al. (2000), Shchipalov (2000), Churakov et al. (2004)
u_a (J/m^2)	0.11	0.11	Wendler et al. (2010), present study
ρ (g/cm^3)	2.5	2.5	Krasilin et al. (2017), Zahidah et al. (2017)
M (g/mol)	277	258	–

[a] the value is the $Mg(OH)_2$ brucite cell parameter multiplied by 3; [b] (0001) surface of $Mg(OH)_2$ brucite; [c] (111) surface of α-SiO_2 cristobalite; [d] (002) surface of $Al(OH)_3$ gibbsite; [e] see the text for comments regarding the range.

known crystal structures, so the value of 1.51 J/m^2 for the (111) α-SiO_2 surface (Shchipalov, 2000) is taken as a reasonable approximation.

Because of this uncertainty with edge surfaces, the model has difficulty distinguishing confidently between σ_1 and σ_2 numerical values, so the case of $\sigma_1 = \sigma_2 = \sigma_e$ is considered. The edge surfaces are a mixture of metal hydroxide and silica surfaces, so whether they are hydroxylated or not is unclear. The calculation studied the scrolling process in the range of 0.5–3.0 J/m^2 of σ_e values. This range was determined by two arguments. First, all of the above-mentioned reports (Fleming et al. 2000; Shchipalov 2000; Churakov et al. 2004) claimed that σ values of the edge surfaces – $(1\bar{1}00)$ $Mg(OH)_2$, (200) $Al(OH)_3$, and, to some extent, (001) α-SiO_2 – were at least twice as large as those of (0001), (002), and (111) surfaces, respectively. Second, surface dehydroxylation usually increased the specific surface energy; typical σ values of MgO and α-Al_2O_3 were 1.5 and 2.0 J/m^2 (Mackrodt et al. 1987; Evarestov and Bandura 2004).

Finally, estimation of the u_a value using Eq. 17 yielded ~0.11 J/m^2 for both chrysotile ($a = 0.530$ nm, $b = 0.922$ nm) (Krasilin et al. 2017) and halloysite (a = 0.513 nm, b = 0.879 nm) (Zhang et al. 2011) layers at 5–6 hydrogen bonds per cell.

By substituting the parameters from Table 1 into Eqs 1 and 13, the energy effects of multi-walled scroll or plate formation were evaluated. In the calculation, the spiral length L_1 varied from 10 nm to 2 μm with a 5 nm step, whereas length L_2 was fixed at 1 μm; in fact, any value could be assigned to L_2 as long as the assumption $\sigma_1 = \sigma_2 = \sigma_e$ was acceptable. For each value of L_1, a local energy minimum was found by changing n with a 0.1 step in correlation with r_{in} (or by changing k with a 1 step in the case of plate formation, see Fig. 1c). This set of points then formed the energy-effect curve represented in Fig. 2a,b.

The Young's modulus and specific surface energy of the octahedral sheet (σ_{out} or σ_{in}) were varied in order to show their influence on the preferred size parameters of chrysotile and halloysite nanoscrolls. Meanwhile, one value was varied and the rest were fixed in correspondence with Table 1. The results are shown in Fig. 2c–f.

RESULTS AND DISCUSSION

Preferred Size Parameters of Chrysotile and Halloysite Nanoscrolls

During spiral-length increase, both chrysotile and halloysite layers demonstrated energy minima (Fig. 2a,b), which originated from an excess strain energy in the growing spiral. No discrepancy was observed between the inner and outer radii curves at small L_1, because curved layers with $n \leq 1$ were more energy effective than multi-walled structures. Preferred size parameters for chrysotile nanoscrolls were: inner radius = 1.9 nm, outer radius = 6.6 nm, 7–8 layers; for halloysite they were: inner radius = 3.2 nm, outer radius = 17.5 nm, 21–22 layers. Surface-energy differences on the opposite side of the layer in the case of chrysotile favored scrolling, whereas in the case of the halloysite layer bending the layer, in the opposite direction was the tendency (Krasilin and Gusarov 2014). That is why the energy minimum of the latter was shallower and wider than that of chrysotile. The position and form of energy minima did not depend on the σ_e value, because the corresponding terms in Eqs 9 and 11 were reduced by subtraction.

In contrast with previous modeling by Krasilin et al. (2017), some of the model parameters (in particular σ_{out}, σ_{in}, and u_a) responsible for the surface and adhesion energy components were essentially changed. These changes did not affect the modeling results qualitatively, but they yielded a new quantitative estimate of the value of the energy effects.

Variation of the Young's modulus value (Fig. 2c,d) and specific surface energy of the octahedral sheet (Fig. 2e,f) had opposing effects on the chrysotile and halloysite preferred radii of curvature. This was probably related to differences in the strain and surface-energy components: in the case of chrysotile layers these two directions are the same whereas in the

https://doi.org/10.1007/s42860-020-00086-6 Published online by Cambridge University Press

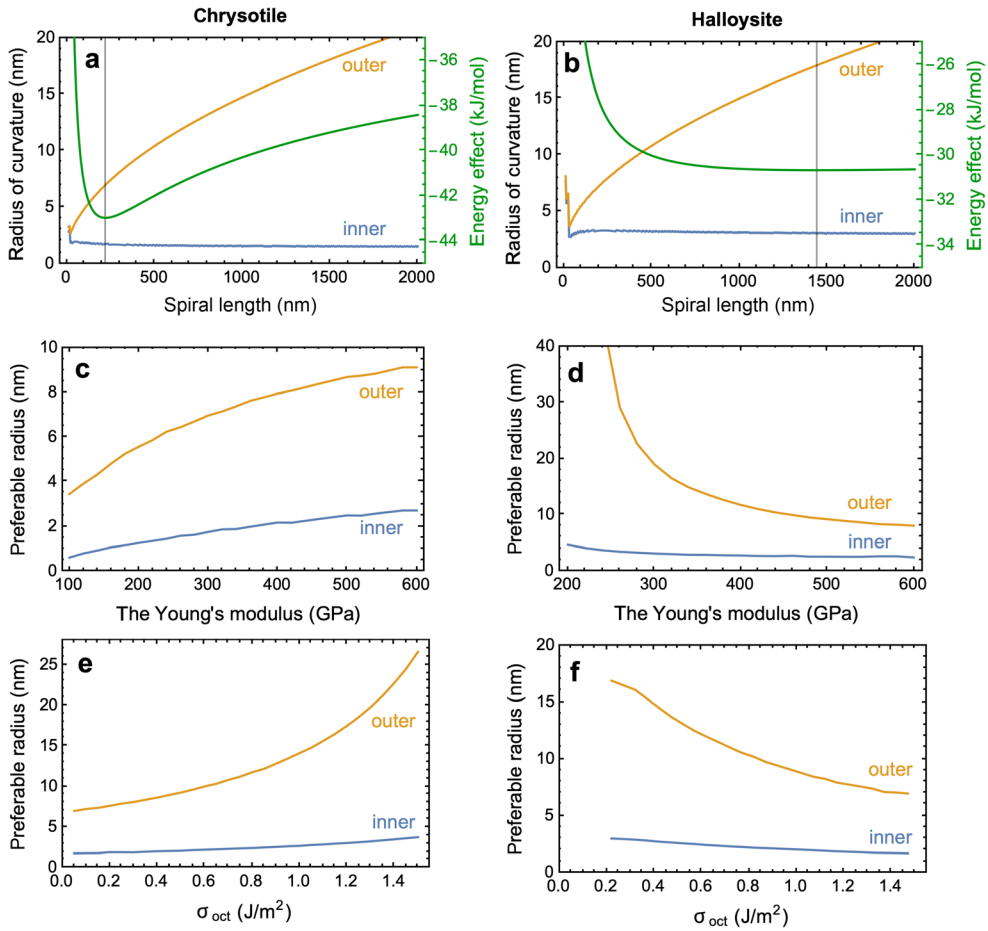

Fig. 2. Preferred size parameters (inner and outer radii of curvature) and energy effect of scrolling ($\Delta E_{/}^{@}$) of **a** chrysotile and **b** halloysite layers. The position of the principal energy minimum is marked by a vertical line. Influence of Young's modulus on **c** chrysotile and **d** halloysite preferred radii of curvature. Influence of the specific surface energy value of the octahedral sheet (σ_{oct}, which is equal to σ_{out} or σ_{in}) on **e** chrysotile and **f** halloysite preferred radii of curvature

case of halloysite layers the two directions are opposite. As a result, halloysite layers were more sensitive to parametric variation. Overestimation of the halloysite layer Young's modulus could lead to discrepancies between calculated and experimental values of the radii of curvature. For example, Lvov and Abdullayev (2013) reported the halloysite nanotube inner radius as being in the 2.5–5 nm range and the outer radius being in the 25–50 nm range. Using a Young's modulus value of 250 GPa instead of 300 GPa was sufficient to obtain the reported values.

Another possible reason for the discrepancy is the conditions of formation of the nanoscrolls; these include temperature, pressure, pH, presence of impurities, and other parameters. In the case of synthetic chrysotile and pecoraite (Ni-based structural analog), increases in temperature and pH yielded increases in the number of layers, outer diameter, and length (Korytkova et al. 2011; Bloise et al. 2012; Krasilin et al. 2017) because they caused significant oversaturation by the hydrothermal medium and intense precipitation of the substance on more available nanoscroll side surfaces. Replacement of 72 pm Mg, 53 pm Al, and 26 pm Si by other cations, e.g. by 69 pm Ni (Bloise et al. 2010; Krasilin et al. 2017, 2019a), 61 pm Fe(II), 55 pm Fe(III) (Korytkova et al. 2007; Bloise et al. 2009b), and 39 pm Ge (Perbost et al. 2003; White et al. 2012), with respect to the energy model, would change the r_0 value (see Eqs 2 and 5) and, consequently, the preferred size parameters of the nanoscroll (ionic radii taken from Shannon 1976). In the case of chrysotile, these substitutions increased the r_0 value and the diameters of the particles. In the particular case of Ge substitution for Si in halloysite, the r_0 value decreased, imparting additional stimuli for the layer to scroll. The difference in ionic radii between these cations is rather large, however, and this led to formation of Ge-doped imogolite nanotubes at high Ge content, as observed by White et al. (2012). The 42 pm Ti content in doped chrysotile nanoscrolls (Bloise et al. 2009a; Maslennikova and Gatina 2018) is limited for the same reason.

Scroll vs Plate

The energy effect of scrolling ($\Delta E_{/}^{@}$) and the energy effect of multi-layered plate formation ($\Delta E_{/}^{=}$) are compared in Fig. 3.

https://doi.org/10.1007/s42860-020-00086-6 Published online by Cambridge University Press

According to Ogorodova et al. (2006), the enthalpies of formation of natural and synthetic chrysotile were 420 kJ/mol and 390 kJ/mol, respectively; so the calculated energy effect of scrolling was at least an order of magnitude weaker (Fig. 3). The comparatively small calculated energy effect of scrolling could explain some difficulties with the experimental observation of the heat effect of scrolling on the background heat effect caused by recrystallization of the starting components (Sharikov et al. 2007).

The specific surface energy of the edges made an essential contribution to $\Delta E_{/}^{=}$. Its decrease favored the initial layer partition and stacking with the formation of a multi-layered structure. As a result, the energy effect of plate formation grew because of the increased contribution of the adhesion energy component (Eq. 16). Due to the absence of the strain energy component in Eq. 13, $\Delta E_{/}^{=}(L_1)$ did not have a minimum, and this prevented determination of the preferred size parameters of that particle. This feature made the platy morphology of the layer less energy preferable than the scrolled morphology for almost the entire range of particle sizes. However, the halloysite layer showed a comparatively small energy gap between scroll and plate, and the latter can be even more preferable at small σ_e and small spiral length L_1 (particle size).

A closer look at the $L_1 = 20..100$ nm region is provided in Fig. 4. At the spiral length $L_1 = 20$ nm (length of a single layer) and with small specific surface energy at the edges, $\sigma_e = 0.5$ J/m^2, the halloysite layer much preferred to form a two-layered 10 nm plate than to scroll, because the total effect of adhesion (Eq. 16) exceeded the effect of edge surface area increase (Eq. 15). The length $L_1 = 30$ nm was already sufficient for the halloysite layer to form a nanoscroll of $n \approx 1.5$, and the energy curve was composed of two overlapping minima due to the contribution of adhesion energy. But this contribution was still insufficient to make the halloysite scroll geometry more energy preferable than the plate, unless the size of the layer reached some critical value, in this case 50 nm.

If the L_1 value increase is considered to be nanoparticle growth during synthesis by adding a portion of substance to the system, then the calculation results shown in Fig. 4 highlight a substantial kinetic hindrance for a layer with a halloysite structure to form a nanoscroll at a given set of parameters. Initial precipitation of additional substance occurred on some of the particle surfaces proportionally to their area (Ivanov et al. 2014), and this feature prevented the growth of one long layer. Later, when length L_1 reached 100 nm, for example, how could the halloysite plate that has already been formed turn into the more energy-preferred nanoscroll? Within the current approximation, only two options exist: full recrystallization of the plate, which would require the presence of additional nuclei in the system, or scrolling of the outer layer of the plate. The latter has been under consideration by Chivilikhin et al. (2007). Here, the actual size of the layer of the 5-layered plate was only 20 nm, and this was insufficient to form a scroll. Even if the plate were larger, the outer layer would need some external stimuli to overcome hydrogen bonding. Use of an intercalation agent that would weaken the adhesion would be such a stimulus (Kuroda et al. 2011).

An important remark regarding the form of the real cross-section should be considered. The curling process could yield both nanoscrolls and nanotubes in some ratio, which, to date, is unknown for chrysotile and halloysite. On the contrary, single- and double-walled imogolites are known to exist as nanotubes, although Thill et al. (2012) reported that multi-walled nanoscrolls of Ge-doped imogolite are a possible exception. The model presented was constructed involving spiral forms of cross sections because otherwise one had to find the energy effect of nanotube formation by solving equations with sums instead of integrals (Belloni and Thill 2016). Assuming that the main contribution is related to the joining of two edge surfaces, the energy effect of nanotube formation instead of a nanoscroll could be estimated as follows:

$$\Delta\Sigma_{/}^{\circledcirc} = -\frac{2\sigma_2 L_2 h}{\nu} = -\frac{2M\sigma_2}{L_1\rho} \tag{18}$$

The value was inversely proportional to the spiral length, so for multi-walled particles the effect was expected to be negligible. In the case of the calculation represented in Fig. 4, this effect could be taken into account by some natural n values. If $L_1 = 20$ nm, the effect would be –5.5 kJ/mol. This would put a total energy effect at $n = 1$ down to –3 kJ/mol (Fig. 4). At L_1 equal to 30 and 50 nm the effects would be –3.7 and –2.2 kJ/mol, respectively. An addition of these values to the points at $n = 1$ and $n = 2$ did not change the conclusion about the energy preference of platy particles.

For real systems containing a large number of particles, other factors can govern their morphology. An ensemble of imogolite nanoparticles, which have the largest strain compared with halloysite and chrysotile, can still be composed of proto-imogolite (particles with $n \ll 1$) if their concentration in the solution is below a certain threshold, according to Belloni and Thill (2016). Despite the fact that the model is focused on comparison of only two particles, it is related indirectly to the possible presence of a concentration threshold. Comparing energy curves at $L_1 = 20$ nm and $L_1 = 30$ nm (Fig. 4), two energy minima can be seen in the $n < 1$ and $n > 1$ areas divided by a barrier at $n = 1$. This means that the particle contained insufficient amounts of substance to form a scroll and it needed to gain it via recrystallization or oriented attachment with adjacent particles, which, in turn, depended on the parameters of the medium, including volume concentration. The $n < 1$ minimum itself is an additional hindrance to multi-walled nanoscroll formation.

The calculated results could be related to the experimental features in the preparation of the initial composition and to the hydrothermal treatment conditions needed to synthesize pure halloysite nanoscrolls. An increase in the σ_e value (Fig. 3) could avoid the platy particle growth demonstrated in Fig. 4 and could probably be achieved by varying the composition of

https://doi.org/10.1007/s42860-020-00086-6 Published online by Cambridge University Press

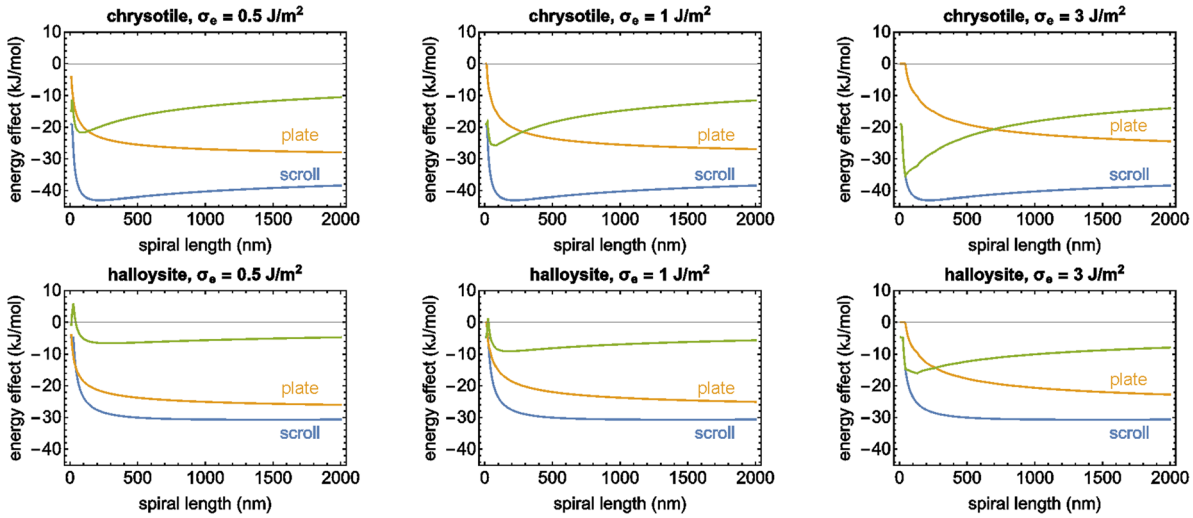

Fig. 3. Energy effect of scrolling ($\Delta E_f^{@}$), formation of a multi-layered plate ($\Delta E_f^{=}$), and the difference curve

the hydrothermal medium, as well as by dehydration of the initial composition by heat treatment, because (see discussion of Table 1) oxide surfaces have a larger σ than hydroxide surfaces. Dehydration should also decrease differences in σ on the opposite sides of the layer, which, in the case of halloysite, hinders scrolling. In addition, the components of the initial composition should be put in chemical contact, instead of using mechanical mixtures of Al_2O_3 and SiO_2, because recrystallization under hydrothermal conditions is usually accompanied by hydration (Korytkova et al. 2004, 2007; Ogorodova et al. 2007).

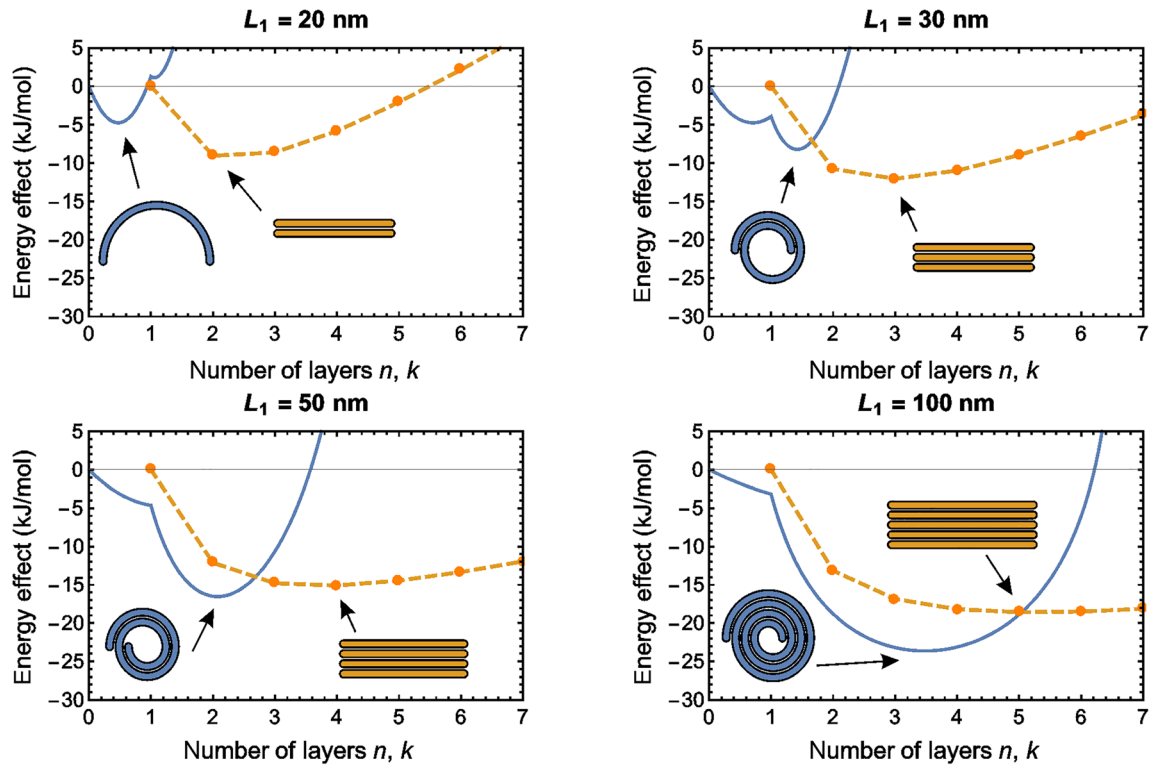

Fig. 4. Energy effect of scrolling ($\Delta E_f^{@}$) and formation of a multi-layered plate ($\Delta E_f^{=}$) vs. the number of layers (n, k) in the case of halloysite with $\sigma_e = 0.5$ J/m^2. The points denoting the energy effect of plate formation are joined by a dashed line for the sake of clarity. The insets show the approximate geometry of the cross sections of the particles

https://doi.org/10.1007/s42860-020-00086-6 Published online by Cambridge University Press

CONCLUSIONS

The aim of the present study was to consider the question, from the perspective of energy modeling, "why do synthetic chrysotile layers form nanoscrolls with ease, whereas halloysite layers tend to form plates?" Analysis of the size mismatch between the sheets has shown that the halloysite layer had even greater scrolling potential than that of chrysotile (the radii of the mechanically unstressed layers were 3.3 nm and 8.8 nm, respectively). These two layers had opposite directions of scrolling, however, and the surface-energy difference on the opposite sides of the halloysite layers acted against the strain-energy component. This was the reason for the striking difference between the preferred size parameters of chrysotile (7–8 layers) and halloysite (21–22 layers) nanoscrolls. Moreover, the sufficiently low specific surface energy of the halloysite edge surfaces enabled the formation of a multi-layered plate instead of a nanoscroll. An halloysite particle 'chose' to be a plate or to scroll at the very beginning of the growth process, and changing the morphology later, in spite of the energy gap between plate and scroll states, was difficult.

ACKNOWLEDGMENTS

The research was supported by the Russian Science Foundation Grant 16-13-10252. The author thanks E.K. Khrapova, Dr T.P. Maslennikova, and Prof. V.V. Gusarov for fruitful discussions.

Compliance with Ethical Standards

Conflict of Interest

The corresponding author states that there is no conflict of interest.

REFERENCES

Arancibia-Miranda, N., Escudey, M., Ramírez, R., González, R.I., van Duin, A.C.T., & Kiwi, M. (2017). Advancements in the synthesis of building block materials: experimental evidence and modeled interpretations of the effect of Na and K on imogolite synthesis. *The Journal of Physical Chemistry C*, *121*, 12658–12668.

Belloni, L. & Thill, A. (2016). Why a 1:1 2D structure tends to roll? A thermodynamic perspective. Pp. 361–386 in: *Nanosized Tubular Clay Minerals: Halloysite and Imogolite* (P. Yuan, A. Thill, and F. Bergaya, editors). Volume 7, Elsevier, Amsterdam.

Berthonneau, J., Grauby, O., Jeannin, C., Chaudanson, D., Joussein, E., & Baronnet, A. (2015). Native morphology of hydrated spheroidal halloysite observed by environmental transmission electron microscopy. *Clays and Clay Minerals*, *63*, 368–377.

Bian, Z. & Kawi, S. (2020). Preparation, characterization and catalytic application of phyllosilicate: A review. *Catalysis Today*, *339*, 3–23.

Bloise, A., Barrese, E., & Apollaro, C. (2009a). Hydrothermal alteration of Ti-doped forsterite to chrysotile and characterization of the resulting chrysotile fibers. *Neues Jahrbuch für Mineralogie – Abhandlungen*, *185*, 297–304.

Bloise, A., Belluso, E., Barrese, E., Miriello, D., & Apollaro, C. (2009b). Synthesis of Fe-doped chrysotile and characterization of the resulting chrysotile fibers. *Crystal Research and Technology*, *44*, 590–596.

Bloise, A., Belluso, E., Fornero, E., Rinaudo, C., Barrese, E., & Capella, S. (2010). Influence of synthesis conditions on growth of Ni-doped chrysotile. *Microporous and Mesoporous Materials*, *132*, 239–245.

Bloise, A., Belluso, E., Catalano, M., Barrese, E., Miriello, D., & Apollaro, C. (2012). Hydrothermal alteration of glass to chrysotile. *Journal of the American Ceramic Society*, *95*, 3050–3055.

Cataldo, S., Lazzara, G., Massaro, M., Muratore, N., Pettignano, A., & Riela, S. (2018). Functionalized halloysite nanotubes for enhanced removal of lead(II) ions from aqueous solutions. *Applied Clay Science*, *156*, 87–95.

Cavallaro, G., Danilushkina, A., Evtugyn, V., Lazzara, G., Milioto, S., Parisi, F., Rozhina, E., & Fakhrullin, R. (2017). Halloysite nanotubes: controlled access and release by smart gates. *Nanomaterials*, *7*, 199.

Chivilikhin, S.A., Popov, I.Y., & Gusarov, V.V. (2007). Dynamics of nanotube twisting in a viscous fluid. *Doklady Physics*, *52*, 60–62.

Chivilikhin, S.A., Popov, I.Y., Svitenkov, A.I., Chivilikhin, D.S., & Gusarov, V.V. (2009). Formation and evolution of nanoscroll ensembles based on layered-structure compounds. *Doklady Physics*, *54*, 491–493.

Churakov, S.V., Iannuzzi, M., & Parrinello, M. (2004). Ab Initio study of dehydroxylation−carbonation reaction on brucite surface. *The Journal of Physical Chemistry B*, *108*, 11567–11574.

Cravero, F., Fernández, L., Marfil, S., Sánchez, M., Maiza, P., & Martínez, A. (2016). Spheroidal halloysites from Patagonia, Argentina: some aspects of their formation and applications. *Applied Clay Science*, *131*, 48–58.

Cressey, B.A. & Whittaker, E.J.W. (1993). Five-fold symmetry in chrysotile asbestos revealed by transmission electron microscopy. *Mineralogical Magazine*, *57*, 729–732.

da Silva, M.C., dos Santos, E.C., Lourenço, M.P., Gouvea, M.P., & Duarte, H.A. (2015). Structural, electronic, and mechanical properties of inner surface modified imogolite nanotubes. *Frontiers in Materials*, *2*, 1–10.

Demichelis, R., De La Pierre, M., Mookherjee, M., Zicovich-Wilson, C.M., & Orlando, R. (2016). Serpentine polymorphism: a quantitative insight from first-principles calculations. *CrystEngComm*, *18*, 4412–4419.

Desgranges, L., Calvarin, G., & Chevrier, G. (1996). Interlayer interactions in $M(OH)_2$: a neutron diffraction study of $Mg(OH)_2$. *Acta Crystallographica Section B: Structural Science*, *52*, 82–86.

Du, P., Thill, A., Yuan, P., Wang, S., Liu, D., Gobeaux, F., Deng, L., & Song, Y. (2020). Tailoring structure and surface chemistry of hollow allophane nanospheres for optimization of aggregation by facile methyl modification. *Applied Surface Science*, *510*, 145453.

Dumitrică, T., Landis, C.M., & Yakobson, B.I. (2002). Curvature-induced polarization in carbon nanoshells. *Chemical Physics Letters*, *360*, 182–188.

Evarestov, R.A. & Bandura, A.V. (2004). HF and DFT calculations of MgO surface energy and electrostatic potential using two- and three-periodic models. *International Journal of Quantum Chemistry*, *100*, 452–459.

Ferrante, F., Armata, N., & Lazzara, G. (2015). Modeling of the halloysite spiral nanotube. *The Journal of Physical Chemistry C*, *119*, 16700–16707.

Fleming, S., Rohl, A., Lee, M.-Y., Gale, J., & Parkinson, G. (2000). Atomistic modelling of gibbsite: surface structure and morphology. *Journal of Crystal Growth*, *209*, 159–166.

Goda, E.S., Gab-Allah, M.A., Singu, B.S., & Yoon, K.R. (2019). Halloysite nanotubes based electrochemical sensors: A review. *Microchemical Journal*, *147*, 1083–1096.

González, R.I., Valencia, F.J., Rogan, J., Valdivia, J.A., Sofo, J., Kiwi, M., & Munoz, F. (2018). Bending energy of 2D materials: graphene, MoS_2 and imogolite. *RSC Advances, 8*, 4577–4583.

Guimarães, L., Enyashin, A.N., Seifert, G., & Duarte, H.A. (2010). Structural, electronic, and mechanical properties of single-walled halloysite nanotube models. *The Journal of Physical Chemistry C*, *114*, 11358–11363.

Holec, D., Dumitraschkewitz, P., Vollath, D., & Fischer, F.D. (2020). Surface energy of Au nanoparticles depending on their size and shape. *Nanomaterials*, *10*, 484.

Ivanov, V.K., Fedorov, P.P., Baranchikov, A.Y., & Osiko, V.V. (2014). Oriented attachment of particles: 100 years of investigations of non-classical crystal growth. *Russian Chemical Reviews*, *83*, 1204–1222.

Korytkova, E.N., Maslov, A.V., Pivovarova, L.N., Drozdova, I.A., & Gusarov, V.V. (2004). Formation of $Mg_3Si_2O_5(OH)_4$ nanotubes under hydrothermal conditions. *Glass Physics and Chemistry*, *30*, 51–55.

Korytkova, E.N., Pivovarova, L.N., Semenova, O.E., Drozdova, I.A., Povinich, V.F., & Gusarov, V.V. (2007). Hydrothermal synthesis of nanotubular Mg-Fe hydrosilicate. *Russian Journal of Inorganic Chemistry*, *52*, 338–344.

Korytkova, E.N., Brovkin, A.S., Maslennikova, T.P., Pivovarova, L.N., & Drozdova, I.A. (2011). Influence of the physicochemical parameters of synthesis on the growth of nanotubes of the $Mg_3Si_2O_5(OH)_4$ composition under hydrothermal conditions. *Glass Physics and Chemistry*, *37*, 161–171.

Krasilin, A.A. & Gusarov, V.V. (2014). Energy of formation of chrysotile nanotubes. *Russian Journal of General Chemistry*, *84*, 2359–2363.

Krasilin, A.A. & Gusarov, V.V. (2015). Energy model of bilayer nanoplate scrolling: Formation of chrysotile nanoscroll. *Russian Journal of General Chemistry*, *85*, 2238–2241.

Krasilin, A.A. & Gusarov, V.V. (2016). Energy model of radial growth of a nanotubular crystal. *Technical Physics Letters*, *42*, 55–58.

Krasilin, A.A. & Gusarov, V.V. (2017). Redistribution of Mg and Ni cations in crystal lattice of conical nanotube with chrysotile structure. *Nanosystems: Physics, Chemistry, Mathematics*, *8*, 620–627.

Krasilin, A.A., Suprun, A.M., Nevedomsky, V.N., & Gusarov, V.V. (2015). Formation of conical $(Mg,Ni)_3Si_2O_5(OH)_4$ nanoscrolls. *Doklady Physical Chemistry*, *460*, 42–44.

Krasilin, A.A., Nevedomsky, V.N., & Gusarov, V.V. (2017). Comparative energy modeling of multiwalled $Mg_3Si_2O_5(OH)_4$ and $Ni_3Si_2O_5(OH)_4$ nanoscroll growth. *The Journal of Physical Chemistry C*, *121*, 12495–12502.

Krasilin, A.A., Khrapova, E.K., Nominé, A., Ghanbaja, J., Belmonte, T., & Gusarov, V.V. (2019a). Cation redistribution along the spiral of Ni-doped phyllosilicate nanoscrolls: energy modelling and STEM/EDS study. *ChemPhysChem*, *20*, 719–726.

Krasilin, A.A., Danilovich, D.P., Yudina, E.B., Bruyere, S., Ghanbaja, J., & Ivanov, V.K. (2019b). Crystal violet adsorption by oppositely twisted heat-treated halloysite and pecoraite nanoscrolls. *Applied Clay Science*, *173*, 1–11.

Kuroda, Y., Ito, K., Itabashi, K., & Kuroda, K. (2011). One-step exfoliation of kaolinites and their transformation into nanoscrolls. *Langmuir*, *27*, 2028–2035.

Lafay, R., Fernandez-Martinez, A., Montes-Hernandez, G., Auzende, A.L., & Poulain, A. (2016). Dissolution-reprecipitation and self-assembly of serpentine nanoparticles preceding chrysotile formation: Insights into the structure of proto-serpentine. *American Mineralogist*, *101*, 2666–2676.

Landau, L.D., Pitaevskii, L.P., Kosevich, A.M., & Lifshitz, E.M. (1986). *Theory of Elasticity, third edition: Volume 7 (course of theoretical physics)*. Oxford, UK: Butterworth-Heinemann, Elsevier.

Lecouvet, B., Horion, J., D'Haese, C., Bailly, C., & Nysten, B. (2013). Elastic modulus of halloysite nanotubes. *Nanotechnology*, *24*, 105704.

Li, X., Wang, D., Liu, Q., & Komarneni, S. (2019). A comparative study of synthetic tubular kaolinite nanoscrolls and natural halloysite nanotubes. *Applied Clay Science*, *168*, 421–427.

Liu, Q., Li, X., & Cheng, H. (2016). Insight into the self-adaptive deformation of kaolinite layers into nanoscrolls. *Applied Clay Science*, *124–125*, 175–182.

López-Salinas, E., Toledo-Antonio, J.A., Manríquez, M.E., Sánchez-Cantú, M., Cruz Ramos, I., & Hernández-Cortez, J.G. (2019). Synthesis and catalytic activity of chrysotile-type magnesium silicate nanotubes using various silicate sources. *Microporous and Mesoporous Materials*, *274*, 176–182.

Lourenço, M.P., de Oliveira, C., Oliveira, A.F., Guimarães, L., & Duarte, H.A. (2012). Structural, electronic, and mechanical properties of single-walled chrysotile nanotube models. *The Journal of Physical Chemistry C*, *116*, 9405–9411.

Lvov, Y, Abdullayev, E. (2013). Functional polymer–clay nanotube composites with sustained release of chemical agents. *Progress in Polymer Science*, *38*, 1690–1719.

Lvov, Y., Wang, W., Zhang, L., & Fakhrullin, R. (2016). Halloysite clay nanotubes for loading and sustained release of functional compounds. *Advanced Materials*, *28*, 1227–1250.

Lvov, Y., Panchal, A., Fu, Y., Fakhrullin, R., Kryuchkova, M., Batasheva, S., Stavitskaya, A., Glotov, A., & Vinokurov, V. (2019). Interfacial self-assembly in halloysite nanotube composites. *Langmuir*, *35*, 8646–8657.

Ma, W., Wu, H., Higaki, Y., & Takahara, A. (2018). Halloysite nanotubes: Green nanomaterial for functional organic-inorganic nanohybrids. *The Chemical Record*, *18*, 986–999.

Mackrodt, W.C., Davey, R.J., Black, S.N., & Docherty, R. (1987). The morphology of α-Al_2O_3 and α-Fe_2O_3: The importance of surface relaxation. *Journal of Crystal Growth*, *80*, 441–446.

Makó, É., Kovács, A., Antal, V., & Kristóf, T. (2017). One-pot exfoliation of kaolinite by solvothermal cointercalation. *Applied Clay Science*, *146*, 131–139.

Maslennikova, T.P. & Gatina, E.N. (2017). Modification of $Mg_3Si_2O_5(OH)_4$ nanotubes by magnetite nanoparticles. *Glass Physics and Chemistry*, *43*, 257–262.

Maslennikova, T.P. & Gatina, E.N. (2018). Hydrothermal synthesis of Ti-doped nickel hydrosilicates of various morphologies. *Russian Journal of Applied Chemistry*, *91*, 286–291.

Momma, K. and Izumi, F. (2011). VESTA 3 for three-dimensional visualization of crystal, volumetric and morphology data. *Journal of Applied Crystallography*, *44*, 1272–1276.

Ogorodova, L.P., Kiseleva, I.A., Korytkova, E.N., & Gusarov, V.V. (2006). The enthalpies of formation of natural and synthetic nanotubular chrysotile. *Russian Journal of Physical Chemistry*, *80*, 1021–1024.

Ogorodova, L.P., Kiseleva, I.A., Korytkova, E.N., & Gusarov, V.V. (2007). Calorimetric investigation of nanotubular hydrosilicates in the $Mg_3Si_2O_5(OH)_4$-$Ni_3Si_2O_5(OH)_4$ system. *Glass Physics and Chemistry*, *33*, 303–305.

Paineau, E., Krapf, M.-E.M., Amara, M.-S., Matskova, N.V., Dozov, I., Rouzière, S., Thill, A., Launois, P., & Davidson, P. (2016). A liquid-crystalline hexagonal columnar phase in highly-dilute suspensions of imogolite nanotubes. *Nature Communications*, *7*, 10271.

Perbost, R., Amouric, M., & Olives, J. (2003). Influence of cation size on the curvature of serpentine minerals: HRTEM-AEM study and elastic theory. *Clays and Clay Minerals*, *51*, 430–438.

Picot, P., Liao, Y., Barruet, E., Gobeaux, F., Coradin, T., & Thill, A. (2018). Exploring hybrid imogolite nanotube formation via Si/Al stoichiometry control. *Langmuir*, *34*, 13225–13234.

Piperno, S., Kaplan-Ashiri, I., Cohen, S.R., Popovitz-Biro, R., Wagner, H.D., Tenne, R., Foresti, E., Lesci, I.G., & Roveri, N. (2007). Characterization of geoinspired and synthetic chrysotile nanotubes by atomic force microscopy and transmission electron microscopy. *Advanced Functional Materials*, *17*, 3332–3338.

Poli, E., Elliott, J.D., Hine, N.D.M., Mostofi, A.A., & Teobaldi, G. (2015). Large-scale density functional theory simulation of inorganic nanotubes: A case study on imogolite nanotubes. *Materials Research Innovations*, *19*, S272–S282.

Poli, E., Elliott, J.D., Ratcliff, L.E., Andrinopoulos, L., Dziedzic, J., Hine, N.D.M., Mostofi, A.A., Skylaris, C.-K., Haynes, P.D., & Teobaldi, G. (2016). The potential of imogolite nanotubes as (co-)photocatalysts: A linear-scaling density functional theory study. *Journal of Physics: Condensed Matter*, *28*, 074003.

Prishchenko, D.A., Zenkov, E.V., Mazurenko, V.V., Fakhrullin, R.F., Lvov, Y.M., & Mazurenko, V.G. (2018). Molecular dynamics of the halloysite nanotubes. *Physical Chemistry Chemical Physics*, *20*, 5841–5849.

Roveri, N., Falini, G., Foresti, E., Fracasso, G., Lesci, I.G., & Sabatino, P. (2006). Geoinspired synthetic chrysotile nanotubes. *Journal of Materials Research*, *21*, 2711–2725.

Saalfeld, H. & Wedde, M. (1974). Refinement of the crystal structure of gibbsite, $Al(OH)_3$. *Zeitschrift für Kristallographie*, *139*, 129–135.

Shafia, E., Esposito, S., Armandi, M., Manzoli, M., Garrone, E., & Bonelli, B. (2016). Isomorphic substitution of aluminium by iron into single-walled alumino-silicate nanotubes: A physico-chemical insight into the structural and adsorption properties of Fe-doped imogolite. *Microporous and Mesoporous Materials*, *224*, 229–238.

Shannon, R.D. (1976). Revised effective ionic radii and systematic studies of interatomic distances in halides and chalcogenides. *Acta Crystallographica Section A*, *32*, 751–767.

Sharikov, F.Y., Korytkova, E.N., & Gusarov, V.V. (2007). Effect of the thermal prehistory of components on the hydration and crystallization of $Mg_3Si_2O_5(OH)_4$ nanotubes under hydrothermal conditions. *Glass Physics and Chemistry*, *33*, 515–520.

Shchipalov, Y.K. (2000). Surface energy of crystalline and vitreous Silica. *Glass and Ceramics*, *57*, 374–377.

Singh, B. (1996). Why does halloysite roll?—A new model. *Clays and Clay Minerals*, *44*, 191–196.

Thill, A., Guiose, B., Bacia-Verloop, M., Geertsen, V., & Belloni, L. (2012). How the diameter and structure of $(OH)_3Al_2O_3Si_xGe_{1-x}OH$ imogolite nanotubes are controlled by an adhesion versus curvature competition. *The Journal of Physical Chemistry C*, *116*, 26841–26849.

Thill, A., Picot, P., & Belloni, L. (2017). A mechanism for the sphere/tube shape transition of nanoparticles with an imogolite local structure (imogolite and allophane). *Applied Clay Science*, *141*, 308–315.

Tolman, R.C. (1949). The effect of droplet size on surface tension. *The Journal of Chemical Physics*, *17*, 333.

Vollath, D., Fischer, F.D., & Holec, D. (2018). Surface energy of nanoparticles – influence of particle size and structure. *Beilstein Journal of Nanotechnology*, *9*, 2265–2276.

Wendler, K., Thar, J., Zahn, S., & Kirchner, B. (2010). Estimating the hydrogen bond energy. *The Journal of Physical Chemistry A*, *114*, 9529–9536.

White, R.D., Bavykin, D.V., & Walsh, F.C. (2012). Spontaneous scrolling of kaolinite nanosheets into halloysite nanotubes in an aqueous suspension in the presence of GeO_2. *The Journal of Physical Chemistry C*, *116*, 8824–8833.

Zahidah, K.A., Kakooei, S., Ismail, M.C., & Bothi Raja, P. (2017). Halloysite nanotubes as nanocontainer for smart coating application: A review. *Progress in Organic Coatings*, *111*, 175–185.

Zhang, H.L., Lei, X.R., Yan, C.J., Wang, H.Q., Xiao, G.Q., Hao, J.R., Wang, D., & Qiu, X.M. (2011). Analysis on crystal structure of 7Å-halloysite. *Advanced Materials Research*, *415–417*, 2206–2214.

Zsirka, B., Táborosi, A., Szabó, P., Szilágyi, R.K., Horváth, E., Juzsakova, T., Fertig, D., & Kristóf, J. (2017). Surface characterization of mechanochemically modified exfoliated halloysite nanoscrolls. *Langmuir*, *33*, 3534–3547.

(Received 26 March 2020; revised 10 June 2020; AE: Eric Ferrage)